

# CP violation in $H^\pm t$ production at the LHC

E. Christova<sup>1</sup>, H. Eberl<sup>2</sup>, E. Ginina<sup>2</sup>, W. Majerotto<sup>2</sup>

<sup>1</sup>Institute for Nuclear Research and Nuclear Energy, BAS, Sofia 1784, Bulgaria

<sup>2</sup>Institut für Hochenergiephysik der Österreichischen Akademie der Wissenschaften,  
A-1050 Vienna, Austria

E-mails: echristo@inrne.bas.bg, helmut@hephy.oeaw.ac.at,  
eginina@hephy.oeaw.ac.at, majer@hephy.oeaw.ac.at

## Abstract

We study effects of CP violation in the associated production of a charged Higgs boson and a top quark at the LHC,  $pp \rightarrow tH^\pm + X$ . We calculate the CP violating asymmetry between the total cross section for  $H^+$  and  $H^-$  production at next-to-leading order in the minimal supersymmetric standard model (MSSM), and perform a detailed numerical analysis. In the production the asymmetry is of the order of 20%. The asymmetry in the production and any subsequent decay of an on-shell charged Higgs boson is to a good approximation the sum of the asymmetry in the production and the asymmetry in the decay. We consider subsequent decays of  $H^\pm$  to  $tb$ ,  $\nu_\tau\tau^\pm$  and  $Wh^0$ . In the case with  $H^\pm \rightarrow tb$  decay, mainly due to CP violating box graphs with gluino, the asymmetry can go up to  $\sim 12\%$ .

# Contents

<b>1</b>	<b>Introduction</b>	<b>2</b>
<b>2</b>	<b>The subprocess <math>bg \rightarrow tH^\pm</math></b>	<b>4</b>
2.1	$s$ -channel amplitude . . . . .	5
2.2	$t$ -channel amplitude . . . . .	6
2.3	Cross section - parton level . . . . .	7
2.4	CP violating asymmetry - parton level . . . . .	10
<b>3</b>	<b>The LHC process <math>pp \rightarrow tH^\pm + X</math></b>	<b>10</b>
3.1	Cross section . . . . .	10
3.2	CP violating asymmetry . . . . .	11
<b>4</b>	<b><math>H^\pm</math> production and decay at LHC</b>	<b>11</b>
4.1	The subprocess $bg \rightarrow tH^\pm \rightarrow tt'b (t\nu_\tau\tau^\pm; tW^\pm h^0)$ . . . . .	11
4.2	CP violating asymmetry - production and decay . . . . .	12
<b>5</b>	<b>Numerical analysis</b>	<b>13</b>
5.1	Production asymmetry . . . . .	14
5.2	Production and decay asymmetry . . . . .	17
<b>6</b>	<b>Conclusions</b>	<b>23</b>
<b>A</b>	<b>Masses and mixing matrices</b>	<b>23</b>
<b>B</b>	<b>Interaction Lagrangian</b>	<b>24</b>
<b>C</b>	<b>Passarino-Veltman integrals</b>	<b>25</b>

## 1 Introduction

If a charged  $H^\pm$  boson is discovered at LHC or at any future collider, it would be a clear signal for Physics beyond the Standard Model (SM). The next question would be which Physics beyond the SM it is – almost all extensions of the SM contain a larger Higgs sector and inevitably predict the existence of a charged Higgs boson. CP violation (CPV) is a possible tool to disentangle the different charged Higgs bosons. The phenomena of CPV is important also because it is believed that this is the key to our understanding the observed abundance of matter over antimatter. Most extensions of the SM contain possible new sources of CPV through additional CPV phases.

In this note we study CPV in the Minimal Supersymmetric Standard Model (MSSM) with complex couplings, being one of the most promising candidates for

an extension of the SM. In MSSM the additional sources of CPV are the phases of the higgsino mass parameter  $\mu = |\mu|e^{i\phi_\mu}$  in the superpotential, of the gaugino mass parameters  $M_i = |M_i|e^{i\phi_i}$ ,  $i = 1, 2, 3$  and of the trilinear couplings  $A_f = |A_f|e^{i\phi_f}$  (corresponding to a fermion  $f$ ) [1], respectively. (Usually  $M_2$  is made real by redefining the fields.) From the point of view of baryogenesis, one might hope that these phases are large [2]. Although the experimental upper bounds on the electron and neutron electric dipole moments [3] constrain the phase of  $\mu$ ,  $\phi_\mu < \mathcal{O}(10^{-2})$  [4], for a typical supersymmetry mass scale of the order of a few hundred GeV, the phases of the other parameters mentioned above are practically unconstrained. The CPV effects that might arise from the trilinear couplings of the first generation  $A_{u,d,e}$  are relatively small as they are proportional to  $m_{u,d,e}$ . The same argument holds for the second generation. Nevertheless, the trilinear couplings of the third generation  $A_{t,b,\tau}$  can lead to significant CPV effects [5, 6], especially in top quark physics [7].

Recently we studied the effects of CPV in the three possible decay modes of the MSSM's charged Higgs boson into ordinary particles [8, 9, 10, 11, 12]  $H^\pm \rightarrow tb$ ,  $H^\pm \rightarrow \nu\tau^\pm$  and  $H^\pm \rightarrow W^\pm h^0$ , where  $h^0$  is the lightest neutral Higgs boson. Loop corrections induced by the MSSM Lagrangian with complex couplings lead to non zero decay rate asymmetries between the partial decay widths of  $H^+$  and  $H^-$ , which is a clear signal of CPV.

Studying the effects of CPV in the decay  $H^\pm \rightarrow tb$ , we found that these effects can be rather large and reach up to 25% [8]. This is mainly due to the contribution of the loop diagrams with stops and sbottoms, whose couplings are enhanced by the large top quark mass. This motivated our interest in studying CPV also in the production of  $H^\pm$  at LHC (considered previously in [13] and [14]), where the dominant production process is the associated production  $pp \rightarrow H^\pm t + X$ , which proceeds at parton level through the reaction  $bg \rightarrow H^\pm t$  [22]. This process contains the same  $H^\pm tb$  vertex and corresponding loop diagrams as the decay  $H^\pm \rightarrow tb$ , and one would expect that the CPV effects might be of the same magnitude. In addition, in the production process there are box graphs that are of the same order. These contain additional sources of CPV and must also be taken into account.

We assume that the charged Higgs is produced on mass shell and we consider the production and decay processes separately. In this paper we first study CPV in  $H^\pm$  production at the LHC,  $pp \rightarrow H^\pm t + X$ , through bottom-gluon fusion in the framework of the MSSM, with running top and bottom Yukawa couplings. Then we study the CPV asymmetry in the combined process of  $H^\pm$  production and decay into  $tb$  and  $\nu\tau^\pm$ , with CPV in both production and decay. We present a detailed numerical study for the CPV asymmetry induced by vertex, selfenergy and box corrections in the MSSM.

The paper is organized as follows. In the next section we study the subprocess  $bg \rightarrow H^\pm t$  including vertex and selfenergy loop corrections and obtain analytical expressions for the cross section and the CP-asymmetry at parton level. In Section 3 we add the parton distribution functions (PDF's) and obtain the CPV asymmetry

of the  $pp \rightarrow H^\pm t + X$  production process. In Section 4 we obtain the asymmetry in the case of charged Higgs boson production and subsequent decay. Section 5 contains the numerical analysis in the MSSM. We end up with a Conclusion and 3 Appendices, which contain some detailed formulas needed in the analysis.

## 2 The subprocess $bg \rightarrow tH^\pm$

We study the following processes connected by charge conjugation

$$b_r(p_b) + g_\mu^\alpha(p_g) \longrightarrow t_s(p_t) + H^-(p_{H^-}), \quad (1)$$

$$\bar{b}_r(p_{\bar{b}}) + g_\mu^\alpha(p_g) \longrightarrow \bar{t}_s(p_{\bar{t}}) + H^+(p_{H^+}), \quad (2)$$

where  $r, s$  and  $\alpha$  are colour indices,  $r, s = 1, 2, 3; \alpha = 1, \dots, 8$ . In the kinematics of the processes we neglect the bottom mass  $m_b$ , working in the approximation  $m_b^2/m_t^2 \simeq m_b^2/m_W^2 \simeq 0$ . However, we keep  $m_b$  non zero in the Yukawa couplings, where it is multiplied by  $\tan\beta$  or  $\cot\beta$ .

The tree-level process (1) contains two graphs - with exchange of a bottom quark ( $s$ -channel) and with exchange of a top quark ( $t$ -channel), see Fig. 1. The Mandelstam variables are

$$\hat{s} = (p_b + p_g)^2, \quad \hat{t} = (p_t - p_g)^2 = (p_b - p_{H^-})^2. \quad (3)$$

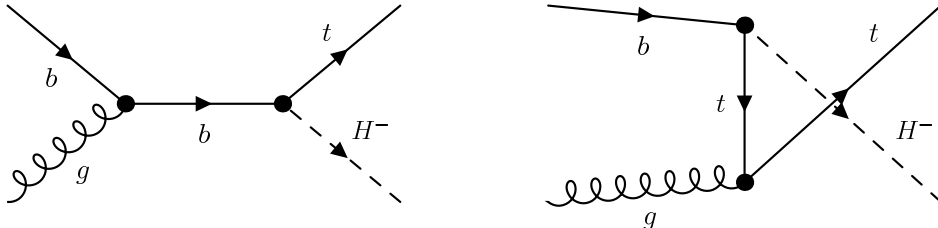


Figure 1: The tree-level graphs of the  $bg \rightarrow tH^-$  process.

At tree-level there is no difference between the cross sections of the considered processes (1) and (2). An asymmetry due to CP non-conservation appears at one-loop level. There are three types of MSSM loop corrections to both  $s$ - and  $t$ -channels that lead to CPV - corrections to the  $H^\pm tb$ -vertex, selfenergy corrections on the  $H^\pm$ -line and box-type corrections, see Fig. 2. The first two types, vertex and selfenergy corrections, are analogous to those in the decay  $H^\pm \rightarrow tb$ . The CPV effects in this decay were studied in [8]. Our analysis in [8] showed that the main contribution to the CPV asymmetry is due to the vertex diagram with a gluino and the  $H^\pm - W^\pm$  selfenergy graph with a  $\tilde{t}\tilde{b}$  loop. These contributions are enhanced by the large top quark mass and the colour factor of 3. The contribution of the rest of the graphs

with supersymmetric particles is negligible. We will present analytical expressions for the vertex correction with  $\tilde{t}\tilde{b}\tilde{g}$  and selfenergy correction with  $\tilde{t}\tilde{b}$  in the loops in the production process. The expressions for the box-diagram contributions are rather lengthy and we do not present them analytically, but in the numerical section they are taken into account.

## 2.1 $s$ -channel amplitude

The matrix element of the graph with bottom exchange on Fig. 1 (the  $s$ -channel), including the vertex correction with a gluino in the  $H^-tb$ -vertex and the  $H^- - W^-$  selfenergy graph with a  $\tilde{t}\tilde{b}$  loop (see Fig. 2) reads<sup>1</sup>

$$\begin{aligned} \mathcal{M}^s = i\frac{g_s}{\hat{s}}\bar{u}_s(p_t) & \left\{ [(y_t + \delta\tilde{Y}_t^s)P_L + (y_b + \delta\tilde{Y}_b^s)P_R](\not{p}_b + \not{p}_g) + \right. \\ & \left. + \hat{s}[f_{RR}^{s,2}P_L + (f_{LL}^{s,2} - \tilde{f}_{LL})P_R] \right\} T_{sr}^\alpha \gamma^\mu u_r(p_b) \epsilon_\mu^\alpha(p_g), \end{aligned} \quad (4)$$

where  $y_t$  and  $y_b$  are the (real) tree-level couplings and the other terms are induced by the loop corrections. The principal difference between the  $bg \rightarrow tH^\pm$  production and the  $H^\pm \rightarrow tb$  decay, considered previously in [8], is in the vertex corrections. In the production process one of the quarks in the  $H^\pm tb$ -vertex is always off-shell - this is the  $b$  quark in the  $s$ -channel and the  $t$  quark in the  $t$ -channel. In the  $H^\pm \rightarrow tb$  decay all particles are on mass shell. This leads to a different structure of the matrix elements. The one-loop form factors of the decay repeat the structure of the tree-level couplings, whereas in the production there are new terms in addition - these terms appear in the second lines of eq. (4) for the  $s$ -channel, and eq. (12) for the  $t$ -channel. For the one-loop form factors in (4) we obtain

$$\delta\tilde{Y}_t^s = m_{\tilde{g}}f_{RL}^{s,0} + m_t(f_{LL}^{s,1} + \tilde{f}_{LL}), \quad \delta\tilde{Y}_b^s = m_{\tilde{g}}f_{LR}^{s,0} + m_t f_{RR}^{s,1}, \quad (5)$$

$$f_{LR}^{s,i} = \frac{2\alpha_s}{3\pi} f_{LR} C_i^s, \quad f_{LR} = \mathcal{R}_{Lm}^{\tilde{t}} \mathcal{R}_{Rn}^{\tilde{b}*} e^{i\phi_{\tilde{g}}}(G_4)_{mn}, \quad (6)$$

$$f_{RL}^{s,i} = \frac{2\alpha_s}{3\pi} f_{RL} C_i^s, \quad f_{RL} = \mathcal{R}_{Rm}^{\tilde{t}} \mathcal{R}_{Ln}^{\tilde{b}*} e^{-i\phi_{\tilde{g}}}(G_4)_{mn}, \quad (7)$$

$$f_{LL}^{s,i} = \frac{2\alpha_s}{3\pi} f_{LL} C_i^s, \quad f_{LL} = \mathcal{R}_{Lm}^{\tilde{t}} \mathcal{R}_{Ln}^{\tilde{b}*}(G_4)_{mn}, \quad (8)$$

$$f_{RR}^{s,i} = \frac{2\alpha_s}{3\pi} f_{RR} C_i^s, \quad f_{RR} = \mathcal{R}_{Rm}^{\tilde{t}} \mathcal{R}_{Rn}^{\tilde{b}*}(G_4)_{mn}, \quad (9)$$

---

<sup>1</sup>In this section details are given on the  $H^-$ -production only.

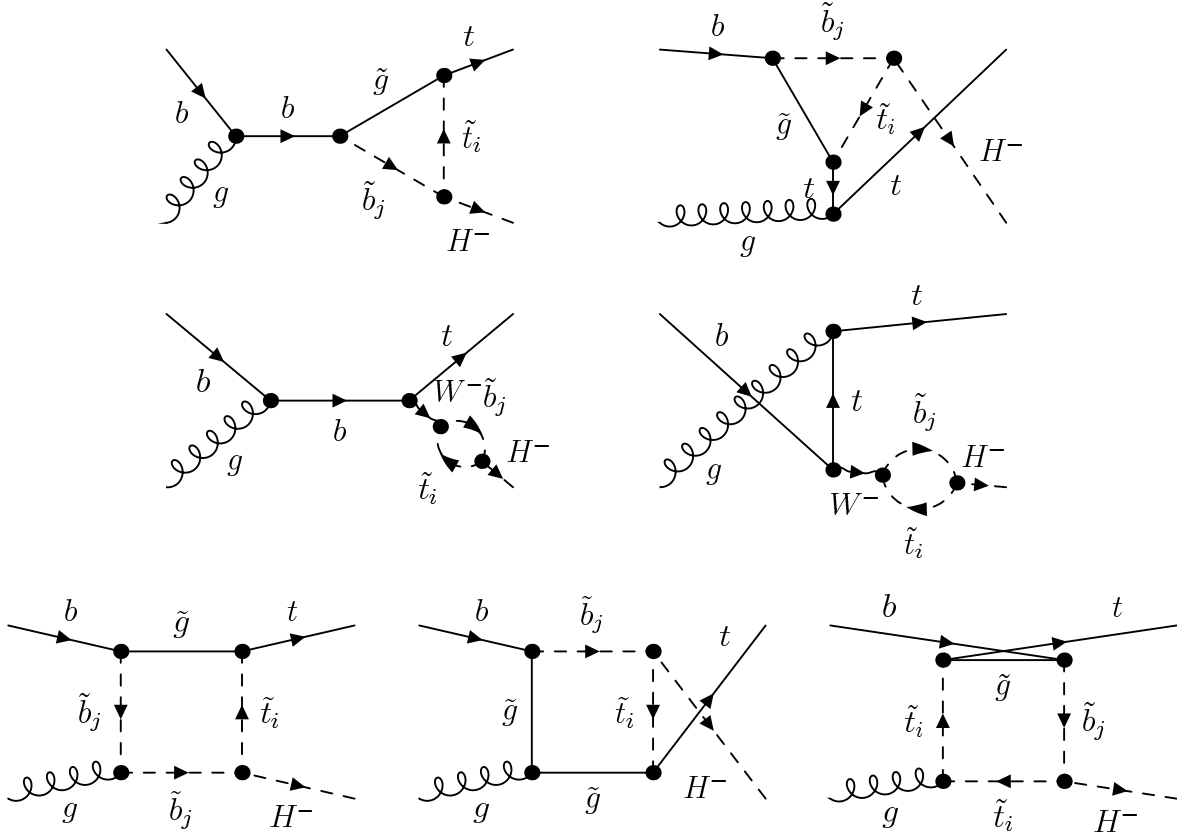


Figure 2: The main sources of CP violation in  $bg \rightarrow H^\pm t$  production.

$$\tilde{f}_{LL} = -\frac{3\alpha_w}{8\pi} \frac{f_{LL}}{m_W^2} (B_0 + 2B_1), \quad (10)$$

where  $\alpha_w = g^2/(4\pi)$  and the arguments of the Passarino-Veltman (PV) integrals are

$$\begin{aligned} C_i^s &= C_i(m_t^2, m_{H^\pm}^2, \hat{s}, m_{\tilde{g}}^2, m_{\tilde{t}_i}^2, m_{\tilde{b}_j}^2), \quad i = 0, 1, 2 \\ B_j &= B_j(m_{H^\pm}^2, m_{\tilde{b}_j}^2, m_{\tilde{t}_i}^2), \quad j = 0, 1. \end{aligned} \quad (11)$$

The full expressions for the mixing matrices, the couplings, as well as the definitions of the PV integrals are given in the Appendices A, B and C, respectively.

## 2.2 $t$ -channel amplitude

The matrix element of the graph with a top exchange ( $t$ -channel) in Fig. 1, including the vertex correction with a gluino in the  $H^-tb$ -vertex and the  $H^- - W^-$  selfenergy graph with a  $\tilde{t}\tilde{b}$  loop (Fig. 2), reads

$$\begin{aligned} \mathcal{M}^t &= i \frac{g_s}{\hat{t} - m_t^2} \bar{u}_s(p_t) \epsilon_\mu^\alpha(p_g) \gamma^\mu T_{sr}^\alpha \left\{ (\not{p}_t - \not{p}_g + m_t) [(y_t + \delta\tilde{Y}_t^t) P_L + (y_b + \delta\tilde{Y}_b^t) P_R] \right. \\ &\quad \left. + (\hat{t} - m_t^2) [(f_{LL}^{t,1} + \tilde{f}_{LL}) P_L + f_{RR}^{t,1} P_R] \right\} u_r(p_b), \end{aligned} \quad (12)$$

where the one-loop form factors are analogous to those of the  $s$ -channel

$$\delta\tilde{Y}_t^t = m_{\tilde{g}} f_{RL}^{t,0} + m_t (f_{LL}^{t,1} + \tilde{f}_{LL}), \quad \delta\tilde{Y}_b^t = m_{\tilde{g}} f_{LR}^{t,0} + m_t f_{RR}^{t,1} \quad (13)$$

$$f_{RL}^{t,i} = f_{RL}^{s,i}(C_i^s \rightarrow C_i^t), \quad \text{etc.}, \quad (14)$$

but with different arguments in the PV integrals

$$C_i^t = C_i(\hat{t}, m_{H^+}^2, m_b^2, m_{\tilde{g}}^2, m_{\tilde{t}}^2, m_b^2), \quad i = 0, 1, 2. \quad (15)$$

## 2.3 Cross section - parton level

In general, the differential cross sections for the processes (1) and (2) are given by

$$d\hat{\sigma}^\pm = \frac{1}{16\pi\hat{s}^2} \frac{1}{96} |\mathcal{M}^\pm|^2 dt, \quad (16)$$

where  $d\hat{\sigma}^\pm$  are averaged (and summed) over initial (and final) colour and spin of all particles of the process, we have used  $\sum_{s,r=1}^3 \sum_{\alpha=1}^8 T_{sr}^\alpha (T_{sr}^{\alpha*}) = 4$ , and the  $\pm$  signs stand for  $H^\pm$  production.

We write the matrix elements of the processes (1) and (2), including the vertex and selfenergy corrections, in the form

$$\mathcal{M}^\pm = \mathcal{M}^{tree,\pm} + \mathcal{M}^{loop,\pm}. \quad (17)$$

Here  $\mathcal{M}^{tree,\pm} = \mathcal{M}_0^{s,\pm} + \mathcal{M}_0^{t,\pm}$  are the tree-level matrix elements (proportional to  $y_t$  and  $y_b$ ), and  $\mathcal{M}^{loop,\pm} = \mathcal{M}_1^{s,\pm} + \mathcal{M}_1^{t,\pm} + \mathcal{M}_2^{s,\pm} + \mathcal{M}_2^{t,\pm}$  are the loop contributions.  $\mathcal{M}_1^{s(t)}$  have the same structure as the tree-level matrix elements and are proportional to  $\delta\tilde{Y}_{t,b}^{s,t}$ .  $\mathcal{M}_2^{s(t)}$  contain the additional terms in (4) and (12). For the squared matrix elements  $|\mathcal{M}^\pm|^2$ , up to terms linear in  $\alpha_s$  and  $\alpha_w$ , we obtain

$$|\mathcal{M}^\pm|^2 = |\mathcal{M}^{tree,\pm}|^2 + 2\text{Re}\left\{ (\mathcal{M}^{tree,\pm})^* \mathcal{M}^{loop,\pm} \right\}. \quad (18)$$

Further, we need to sum over the polarizations of the incoming gluon. At loop level special care must be taken to preserve gauge invariance. We use the axial gauge:

$$\sum_{\lambda=1}^2 \epsilon_\mu^{\alpha*}(k, \lambda) \epsilon_\nu^\beta(k, \lambda) = \delta^{\alpha\beta} \left( -g_{\mu\nu} - \frac{\eta^2 k_\mu k_\nu}{(\eta \cdot k)^2} + \frac{\eta_\mu k_\nu + \eta_\nu k_\mu}{\eta \cdot k} \right), \quad (19)$$

where  $\eta$  is an arbitrary four-vector that fixes the gauge and fulfills  $\eta \cdot \epsilon = 0$  and  $\eta \cdot k \neq 0$ . One can see that in this gauge the unphysical longitudinal degree of freedom manifests itself by an  $\eta$ -dependent polarization sum over the two transverse gluon polarizations. The cross section, being a measurable quantity should be gauge invariant and therefore the  $\eta$ -dependence should ultimately cancel. Using only  $-g_{\mu\nu}$  on the right side of eq. (19) is sufficient at tree-level, because the term resulting from the second and third term on the right side of eq. (19) drops out in the squared matrix element of the sum of the  $s$ - and  $t$ -channels. This is not true anymore at one-loop level because the one-loop factors, e.g.  $\delta\tilde{Y}_{t,b}^s$ , eq. (5), and  $\delta\tilde{Y}_{t,b}^t$ , eq. (13), are different.

For the terms in (18) we obtain

$$\mathcal{M}_0^{s*, -} \mathcal{M}_1^{s, -} = -32\pi\alpha_s(\delta\tilde{Y}_t^s y_t + \delta\tilde{Y}_b^s y_b)[\mathcal{X}_1(\hat{s}, \hat{t}) - 2\mathcal{U}(\hat{s}, \hat{t})c_\eta], \quad (20)$$

$$\mathcal{M}_0^{t*, -} \mathcal{M}_1^{s, -} = -32\pi\alpha_s(\delta\tilde{Y}_t^s y_t + \delta\tilde{Y}_b^s y_b)[\mathcal{X}_{12}(\hat{s}, \hat{t}) + 2\mathcal{U}(\hat{s}, \hat{t})c_\eta + \mathcal{U}(\hat{s}, \hat{t})\mathcal{V}(\hat{s}, \hat{t})], \quad (21)$$

$$\mathcal{M}_0^{s*, -} \mathcal{M}_1^{t, -} = -32\pi\alpha_s(\delta\tilde{Y}_t^t y_t + \delta\tilde{Y}_b^t y_b)[\mathcal{X}_{12}(\hat{s}, \hat{t}) + 2\mathcal{U}(\hat{s}, \hat{t})c_\eta + \mathcal{U}(\hat{s}, \hat{t})\mathcal{V}(\hat{s}, \hat{t})], \quad (22)$$

$$\mathcal{M}_0^{t*, -} \mathcal{M}_1^{t, -} = -32\pi\alpha_s(\delta\tilde{Y}_t^t y_t + \delta\tilde{Y}_b^t y_b)[\mathcal{X}_2(\hat{s}, \hat{t}) - 2\mathcal{U}(\hat{s}, \hat{t})c_\eta - 2\mathcal{U}(\hat{s}, \hat{t})\mathcal{V}(\hat{s}, \hat{t})], \quad (23)$$

$$\mathcal{M}_0^{s*, -} \mathcal{M}_2^{s, -} = 32\pi\alpha_s m_t [(f_{LL}^{s,2} - \tilde{f}_{LL})y_t + f_{RR}^{s,2}y_b][1 + 2c_\eta], \quad (24)$$

$$\mathcal{M}_0^{t*, -} \mathcal{M}_2^{s, -} = 32\pi\alpha_s m_t [(f_{LL}^{s,2} - \tilde{f}_{LL})y_t + f_{RR}^{s,2}y_b][\mathcal{V}(\hat{s}, \hat{t}) - 2c_\eta - \mathcal{V}(\hat{s}, \hat{t})], \quad (25)$$

$$\mathcal{M}_0^{s*, -} \mathcal{M}_2^{t, -} = 32\pi\alpha_s m_t [(f_{LL}^{t,1} + \tilde{f}_{LL})y_t + f_{RR}^{t,1}y_b][1 + 2c_\eta], \quad (26)$$

$$\mathcal{M}_0^{t*, -} \mathcal{M}_2^{t, -} = 32\pi\alpha_s m_t [(f_{LL}^{t,1} + \tilde{f}_{LL})y_t + f_{RR}^{t,1}y_b][\mathcal{V}(\hat{s}, \hat{t}) - 2c_\eta - \mathcal{V}(\hat{s}, \hat{t})]. \quad (27)$$

Here  $\mathcal{X}$ ,  $\mathcal{U}$ ,  $\mathcal{V}$  and  $\mathcal{Y}$ -functions are given by

$$\mathcal{X}_1(\hat{s}, \hat{t}) = \frac{\hat{t} - m_t^2}{\hat{s}}, \quad (28)$$

$$\mathcal{X}_{12}(\hat{s}, \hat{t}) = \frac{(\hat{t} - m_{H^+}^2)(\hat{s} + m_t^2 - m_{H^+}^2) - m_t^2 \hat{s}}{\hat{s}(\hat{t} - m_t^2)}, \quad (29)$$

$$\mathcal{X}_2(\hat{s}, \hat{t}) = \frac{\hat{s}(\hat{t} - m_t^2) + 2m_t^2(\hat{t} - m_{H^+}^2)}{(\hat{t} - m_t^2)^2}, \quad (30)$$

$$\mathcal{U}(\hat{s}, \hat{t}) = \frac{\hat{s} + \hat{t} - m_{H^+}^2}{\hat{s}}, \quad \mathcal{V}(\hat{s}, \hat{t}) = \frac{m_{H^+}^2 - \hat{t}}{\hat{t} - m_t^2}, \quad (31)$$

$$\mathcal{Y}(\hat{s}, \hat{t}) = \frac{\hat{s} + m_{H^+}^2 - \hat{t}}{\hat{t} - m_t^2}. \quad (32)$$



The terms proportional to the number  $c_\eta$  carry the  $\eta$ -dependence. The calculation is done for two specific choices of  $\eta = p_b$ ;  $c_\eta = 0$  and  $\eta = p_b + p_g$ ;  $c_\eta = 1$ . In the center of mass system,  $\vec{p}_b + \vec{p}_g = 0$ , it is easy to see that in both cases the above conditions  $\eta \cdot \epsilon = 0$  and  $\eta \cdot k \neq 0$  are fulfilled. The sum of the products (20) – (27) is independent on  $\eta$  and therefore gauge invariant.

Using eqs. (16) and (18) for the total parton level cross sections of the processes (1) and (2) we obtain

$$\hat{\sigma}^\pm = \hat{\sigma}^{tree} + \frac{1}{8\pi\hat{s}^2} \frac{1}{96} \int_{t_{min}}^{t_{max}} \text{Re} \left\{ (\mathcal{M}^{tree,\pm})^* \mathcal{M}^{loop,\pm} \right\} dt, \quad (33)$$

where the integration limits are given by

$$t_{min,max} = \frac{1}{2}(m_t^2 + m_{H^+}^2 - \hat{s} \mp \lambda^{1/2}(\hat{s}, m_t^2, m_{H^+}^2)), \quad (34)$$

and  $\hat{\sigma}^{tree}$  is the tree-level cross section, which is the same for (1) and (2) [15]

$$\begin{aligned} \hat{\sigma}^{tree}(\hat{s}) &= \frac{\alpha_s}{96\hat{s}^3} (y_t^2 + y_b^2) \left\{ \lambda^{1/2}(\hat{s}, m_t^2, m_{H^+}^2) \left( 7(m_{H^+}^2 - m_t^2) - 3\hat{s} \right) - \right. \\ &\quad \left. - 2 \left( 2(m_{H^+}^2 - m_t^2)^2 - 2(m_{H^+}^2 - m_t^2)\hat{s} + \hat{s}^2 \right) \times \right. \\ &\quad \left. \times \ln \left( \frac{\hat{s} - (m_{H^+}^2 - m_t^2) - \lambda^{1/2}(\hat{s}, m_t^2, m_{H^+}^2)}{\hat{s} - (m_{H^+}^2 - m_t^2) + \lambda^{1/2}(\hat{s}, m_t^2, m_{H^+}^2)} \right) \right\}. \end{aligned} \quad (35)$$

We write the cross sections of the conjugate processes  $\hat{\sigma}^\pm$  given with (33) as a sum of CP invariant and CP violating parts

$$\hat{\sigma}^\pm = \hat{\sigma}^{inv} \pm \hat{\sigma}^{CP}, \quad (36)$$

where the CPV part  $\hat{\sigma}^{CP}$  is given by

$$\begin{aligned} \hat{\sigma}^{CP} &= \frac{\alpha_s}{24\hat{s}^2} \left\{ \mathcal{A}^s \int_{t_{min}}^{t_{max}} (\mathcal{X}_1 + \mathcal{X}_{12} + \mathcal{UV}) dt \right. \\ &\quad \left. + \int_{t_{min}}^{t_{max}} \mathcal{A}^t (\mathcal{X}_{12} + \mathcal{X}_2 - \mathcal{UV}) dt - \int_{t_{min}}^{t_{max}} (\mathcal{B}^s + \mathcal{B}^t) (1 + \mathcal{Y} - \mathcal{V}) dt \right\}, \end{aligned} \quad (37)$$

with

$$\begin{aligned} \mathcal{A}^{s(t)} &= \frac{2\alpha_s m_{\tilde{g}}}{3\pi} [\text{Im}(f_{RL})y_t + \text{Im}(f_{LR})y_b] \text{Im}(C_0^{s(t)}) + \frac{2\alpha_s m_t}{3\pi} [\text{Im}(f_{LL})y_t + \\ &\quad + \text{Im}(f_{RR})y_b] \text{Im}(C_1^{s(t)}) - \frac{3\alpha_w m_t}{8\pi} \text{Im}(f_{LL})y_t \frac{\text{Im}(B_0 + 2B_1)}{m_W^2}, \end{aligned} \quad (38)$$

$$\mathcal{B}^{s(t)} = \frac{2\alpha_s m_t}{3\pi} [\text{Im}(f_{LL})y_t + \text{Im}(f_{RR})y_b] \text{Im}(C_{2(1)}^{s(t)}), \quad (39)$$

and the CP conserving part  $\hat{\sigma}^{inv}$  can be expressed in terms of  $\hat{\sigma}^{CP}$  with exchanging the imaginary parts of the couplings and the PV integrals with real ones

$$\hat{\sigma}^{inv} = \hat{\sigma}^{tree} - \hat{\sigma}^{CP} \text{ (with Im} \rightarrow \text{Re)}. \quad (40)$$

## 2.4 CP violating asymmetry - parton level

We define the CPV asymmetry at parton level as the difference between the total number of produced  $H^+$  and  $H^-$  in bottom-gluon fusion

$$\hat{A}_P^{CP} = \frac{\hat{\sigma}(\bar{b}g \rightarrow \bar{t}H^+) - \hat{\sigma}(bg \rightarrow tH^-)}{\hat{\sigma}(\bar{b}g \rightarrow \bar{t}H^+) + \hat{\sigma}(bg \rightarrow tH^-)}. \quad (41)$$

Taking into account (36), we obtain

$$\hat{A}_P^{CP} = \frac{\hat{\sigma}^{CP}}{\hat{\sigma}^{inv}} \simeq \frac{\hat{\sigma}^{CP}}{\hat{\sigma}^{tree}}, \quad (42)$$

where  $\hat{\sigma}^{CP}$  and  $\hat{\sigma}^{tree}$  are given by (37) and (35).

## 3 The LHC process $pp \rightarrow tH^\pm + X$

### 3.1 Cross section

We study charged Higgs boson production associated with top quark production in proton-proton collisions

$$p(P_A) + p(P_B) \rightarrow t(p_t) + H^\pm(p_{H^\pm}) + X. \quad (43)$$

The Mandelstam variable is  $S = (P_A + P_B)^2$  ( for LHC  $\sqrt{S} = 14$  TeV). We set  $p_b = x_b P_A = \tilde{x}_b P_B$  and  $p_g = x_g P_B = \tilde{x}_g P_A$ , where  $x_i$  ( $\tilde{x}_i$ ) is the momentum fraction of the hadron  $B(A)$  carried by the parton  $i$ . Neglecting the proton mass compared to  $\sqrt{S}$  we get  $\hat{s} = x_b x_g S = \tilde{x}_b \tilde{x}_g S$ . We have

$$\sigma^-(pp \rightarrow tH^-) = 2 \int_0^1 f_b(x_b) \int_0^1 f_g(x_g) \hat{\sigma}^-(x_b x_g S) \theta(x_b x_g S - S_0) dx_b dx_g, \quad (44)$$

$$\sigma^+(pp \rightarrow \bar{t}H^+) = 2 \int_0^1 f_{\bar{b}}(x_{\bar{b}}) \int_0^1 f_g(x_g) \hat{\sigma}^+(x_{\bar{b}} x_g S) \theta(x_{\bar{b}} x_g S - S_0) dx_{\bar{b}} dx_g. \quad (45)$$

Here  $S_0 = (m_t + m_{H^\pm})^2$  fixes the kinematically allowed energy range, and  $f_b$  and  $f_g$  are the PDF's of the bottom and the gluon in the proton. As  $f_b(x_b) = f_{\bar{b}}(x_{\bar{b}})$ , we obtain

$$\sigma^\pm(pp \rightarrow tH^\pm) = 2 \int_0^1 f_b(x_b) \int_0^1 f_g(x_g) \hat{\sigma}^\pm(x_b x_g S) \theta(x_b x_g S - S_0) dx_b dx_g. \quad (46)$$

The factor 2 in the above expressions counts the two possibilities –  $b$  ( $g$ ) comes from the proton  $A$  ( $B$ ) and *vice versa*.

### 3.2 CP violating asymmetry

We define the CPV asymmetry at hadron level as the difference between the total number of produced  $H^+$  and  $H^-$  in proton-proton collisions

$$A_P^{CP} = \frac{\sigma(pp \rightarrow \bar{t}H^+) - \sigma(pp \rightarrow tH^-)}{\sigma(pp \rightarrow \bar{t}H^+) + \sigma(pp \rightarrow tH^-)}. \quad (47)$$

Taking into account (46) we obtain

$$A_P^{CP} = \frac{\int f_b(x_b)f_g(x_g)(\hat{\sigma}^+ - \hat{\sigma}^-)\theta(x_b x_g S - S_0)dx_b dx_g}{\int f_b(x_b)f_g(x_g)(\hat{\sigma}^+ + \hat{\sigma}^-)\theta(x_b x_g S - S_0)dx_b dx_g}. \quad (48)$$

According to (36), for the CPV asymmetry  $A_P^{CP}$  up to terms linear in  $\alpha_s$  and  $\alpha_w$ , we obtain

$$A_P^{CP} = \frac{\sigma^{CP}}{\sigma^{tree}}, \quad (49)$$

where  $\sigma^{CP}$  is the CPV part of the cross section

$$\sigma^{CP}(pp \rightarrow tH^-) = 2 \int_0^1 f_b(x_b) \int_0^1 f_g(x_g) \hat{\sigma}^{CP}(x_b x_g S) \theta(x_b x_g S - S_0) dx_b dx_g, \quad (50)$$

and  $\sigma^{tree}$  is the tree-level cross section

$$\sigma^{tree}(pp \rightarrow tH^-) = 2 \int_0^1 f_b(x_b) \int_0^1 f_g(x_g) \hat{\sigma}^{tree}(x_b x_g S) \theta(x_b x_g S - S_0) dx_b dx_g. \quad (51)$$

## 4 $H^\pm$ production and decay at LHC

After the charged Higgs is produced in proton-proton collisions it will be identified through some of its decay modes. Here we study the combined processes of  $H^\pm$  production and decay, considering  $H^\pm$  decays into  $tb$ ,  $\nu\tau^\pm$  and  $W^\pm h^0$ .

### 4.1 The subprocess $bg \rightarrow tH^\pm \rightarrow tt'b$ ( $t\nu_\tau\tau^\pm$ ; $tW^\pm h^0$ )

In the narrow width approximation, when the decay width of  $H^\pm$  is much smaller than its mass  $m_{H^\pm}$ , the total cross section for charged Higgs production in  $bg \rightarrow tH^\pm$ , with a subsequent decay  $H^\pm \rightarrow f$ , where  $f$  stands for the chosen decay mode  $f = tb$ ;  $\nu\tau^\pm$  and  $W^\pm h^0$ , is given by

$$\hat{\sigma}_f^\pm = \hat{\sigma}_P(bg \rightarrow tH^\pm) \frac{\Gamma(H^\pm \rightarrow f)}{\Gamma_{H^\pm}}. \quad (52)$$

Here,  $\hat{\sigma}_P$  is the total production cross section,  $\Gamma(H^\pm \rightarrow f) \equiv \Gamma_f^\pm$  is the corresponding partial decay width of  $H^\pm$ , and  $\Gamma_{H^\pm}$  is its total decay width.

We already had the expression for the production parton level cross section  $\hat{\sigma}_P^\pm$  in the form (eq. (36))

$$\hat{\sigma}_P^\pm = \hat{\sigma}_P^{inv} \pm \hat{\sigma}_P^{CP}. \quad (53)$$

The considered partial decay widths of  $H^\pm$ , assuming CPV, were obtained in [8, 9, 10], and we write them in the form

$$\Gamma_f^\pm = \Gamma_0^f \left( \Gamma_f^{inv} \pm \Gamma_f^{CP} \right), \quad (54)$$

where  $\Gamma_f^{inv}$  and  $\Gamma_f^{CP}$  are their CP invariant and CP violating parts.

For the total cross section of  $H^\pm$ -production and decay at parton level, assuming CPV in both production and decay, we obtain

$$\hat{\sigma}_f^\pm = \Gamma_0^f \left[ \hat{\sigma}_P^{inv} \Gamma_f^{inv} \pm \left( \hat{\sigma}_P^{CP} \Gamma_f^{inv} + \Gamma_f^{CP} \hat{\sigma}_P^{inv} \right) \right]. \quad (55)$$

## 4.2 CP violating asymmetry - production and decay

We define the CPV asymmetry in charged Higgs boson production in  $pp \rightarrow tH^\pm$ , with a subsequent decay  $H^\pm \rightarrow f$ , assuming CPV in both production and decay, as

$$A_f^{CP} = \frac{\sigma(pp \rightarrow \bar{t}H^+ \rightarrow \bar{t}f) - \sigma(pp \rightarrow tH^- \rightarrow t\bar{f})}{\sigma(pp \rightarrow \bar{t}H^+ \rightarrow \bar{t}f) + \sigma(pp \rightarrow tH^- \rightarrow t\bar{f})}, \quad (56)$$

where  $f$  stands for the chosen decay mode  $f = t\bar{b}; \nu\tau^+$  and  $W^+h^0$ .

In narrow width approximation, taking into account (52), we get

$$A_f^{CP} = \frac{\sigma_P(pp \rightarrow \bar{t}H^+) \Gamma(H^+ \rightarrow f) - \sigma_P(pp \rightarrow tH^-) \Gamma(H^- \rightarrow \bar{f})}{\sigma_P(pp \rightarrow \bar{t}H^+) \Gamma(H^+ \rightarrow f) + \sigma_P(pp \rightarrow tH^-) \Gamma(H^- \rightarrow \bar{f})}, \quad (57)$$

which leads to [13, 14]

$$A_f^{CP} = \frac{\sigma_P^{inv} \Gamma_f^{CP} + \sigma_P^{CP} \Gamma_f^{inv}}{\sigma_P^{inv} \Gamma_f^{inv}} = \frac{\sigma_P^{CP}}{\sigma_P^{inv}} + \frac{\Gamma_f^{CP}}{\Gamma_f^{inv}} = A_P^{CP} + A_{D,f}^{CP}, \quad (58)$$

*i.e.* when the decay width of  $H^\pm$  is much smaller than its mass  $m_{H^\pm}$ , the total asymmetry  $A_f^{CP}$  is an algebraic sum of the CPV asymmetry  $A_P^{CP}$  in the production, and the CPV asymmetry  $A_{D,f}^{CP}$  in the decay  $f$  of the charged Higgs boson.<sup>2</sup>

---

<sup>2</sup>In [16] the asymmetry  $A_D^{CP}$  in the decay is denoted with  $\delta^{CP}$ .

## 5 Numerical analysis

We present numerical results for the charged Higgs rate asymmetries  $A_P^{CP}$ ,  $A_{tb}^{CP}$  and  $A_{\nu\tau}^{CP}$ , eqs. (47) and (56), in the MSSM. All formulas used in the numerical code are calculated analytically, except for the box contributions, which are rather lengthy. Furthermore, all individual one-loop contributions are checked numerically using the packages FEYNARTS and FORMCALC [17]. We also use LOOPTOOLS, see again [17], and FF [18]. In the numerical code the Yukawa couplings of the third generation quarks ( $h_t$ ,  $h_b$ ) are taken to be running [8], at the scale  $Q = m_{H^+} + m_t$ . For the evaluation of the PDF's of the bottom quark and the gluon,  $f_b$  and  $f_g$ , we use CTEQ6L [19], with leading order PDF's and next-to-leading order  $\alpha_s$ , at the same scale  $Q$ . We assume the grand unified theory relation between  $M_1$  and  $M_2$ , so that the phase of  $M_1 = 0$ . Our numerical study shows that the contributions of the loop diagrams with chargino, neutralino, stau and sneutrino to the considered CPV asymmetries are negligible, and besides one exception we show only the contributions from diagrams with  $\tilde{t}b$  and  $\tilde{g}$ . We start from the following reference scenario:

$$\begin{aligned} \tan\beta = 5, \quad M_2 = 300 \text{ GeV}, \quad m_{\tilde{g}} = 727 \text{ GeV}, \quad M_{\tilde{U}} = M_{\tilde{Q}} = M_{\tilde{D}} = 350 \text{ GeV}, \\ \mu = -700 \text{ GeV}, \quad |A_t| = |A_b| = 700 \text{ GeV}, \quad \phi_{A_t} = \frac{\pi}{2}, \quad \phi_{A_b} = \phi_\mu = \phi_3 = 0. \end{aligned} \quad (59)$$

The relevant masses of the sparticles for this choice of parameters, and also for  $\tan\beta = 30$  are shown in Table 1.

As we will see, in such a scenario the effects of CPV are substantial. It is not one of the commonly used minimal supergravity or constrained MSSM scenarios [20], for which most studies have been done. There exist experimental constraints from  $b \rightarrow s\gamma$ , relic density, etc.. In principle, there are enough free parameters in the general complex MSSM to be compatible with all data.

$\tan\beta$	$m_{\tilde{\chi}_1^0}$	$m_{\tilde{\chi}_2^0}$	$m_{\tilde{\chi}_3^0}$	$m_{\tilde{\chi}_4^0}$	$m_{\tilde{\chi}_1^+}$	$m_{\tilde{\chi}_2^+}$	$m_{\tilde{t}_1}$	$m_{\tilde{t}_2}$	$m_{\tilde{b}_1}$	$m_{\tilde{b}_2}$	$m_{\tilde{\tau}_1}$	$m_{\tilde{\tau}_2}$	$m_{\tilde{\nu}}$
5	142	300	706	706	300	709	166	522	327	377	344	362	344
30	141	296	705	709	296	711	172	519	183	464	295	402	344

Table 1: Masses of the sparticles (in GeV) for the parameter set (59).

In Fig. 3 the tree-level cross section  $\sigma(pp \rightarrow tH^- + X)$  is shown as a function of  $m_{H^+}$ , based only on the parton process  $gb \rightarrow tH^-$ , with on-shell and with running  $h_t$  and  $h_b$ . Taking running  $h_t$  and  $h_b$  reduces  $\sigma^{tree}$  by about  $\sim 30\%$ . For  $m_{H^+} \gtrsim 1000$  GeV the cross section drops below 1 fb.

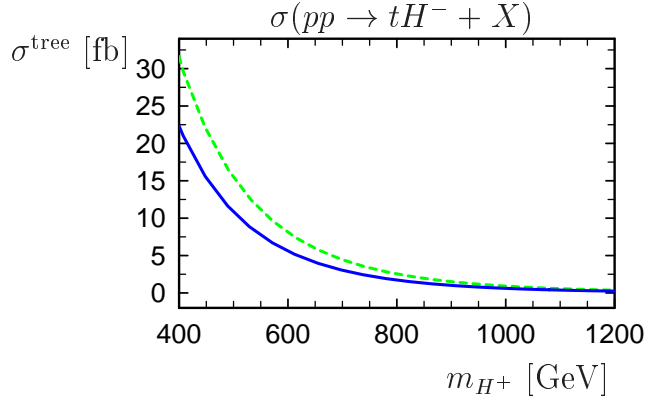


Figure 3: The hadron tree-level cross section for the chosen set of parameters (59) as a function of  $m_{H^+}$ . The green dashed line corresponds to the result using on-shell and the solid blue line to that using running  $h_t$  and  $h_b$ .

## 5.1 Production asymmetry

As expected, the CPV asymmetry in the production due to the loop corrections with  $\tilde{t}\tilde{b}$  and  $\tilde{g}$  is of the same order of magnitude as in the case of the decay  $H^\pm \rightarrow tb$  [8], and can go up to  $\sim 20\%$ . Moreover, the contributions of the box graphs are significant and can be dominant for relatively small  $m_{H^+}$ .

In Fig. 4 the dependence of the different contributions on  $\sqrt{\hat{s}}$  of the underlying parton process  $gb \rightarrow tH^-$  is shown for  $m_{H^+} = 700$  GeV. The kinematical threshold is at  $\sqrt{\hat{s}} = 871.4$  GeV. First the box contribution is the biggest one with a maximum at  $\sim -23\%$ . Then it drops down asymptotically to zero at  $\sqrt{\hat{s}} \gtrsim 1700$  GeV. The vertex contribution has a similar shape with about half of the size of the box contribution. But for  $\sqrt{\hat{s}} > 1500$  GeV it becomes constant being of  $-2\%$ . The selfenergy contribution is independent of  $\sqrt{\hat{s}}$ , about  $-12\%$ . We show it only for completeness. Here also the box and vertex contribution with  $\tilde{\chi}^{0/+}$ , denoted by the pink dash-dotted line, are shown. This contribution is always below  $0.5\%$ , and therefore we will not show it anymore in the figures. The two spikes in the box and in the vertex contributions denote the two thresholds  $\sqrt{\hat{s}} = m_{\tilde{g}} + m_{\tilde{b}_{1,2}}$ , see Table 1.

The contributions of the vertex, selfenergy and box graphs with  $\tilde{t}\tilde{b}$  and  $\tilde{g}$  to the asymmetry  $A_P^{CP}$  at hadron level as functions of  $m_{H^+}$  are shown on Fig. 5. The large effect seen on the figure is mainly due to the phase of  $A_t$ , and the asymmetry reaches its maximum for a maximal phase  $\phi_{A_t} = \pi/2$ . The phase of  $A_b$  does not have a big influence on the asymmetry and therefore we usually set it zero. The four kinks in all three lines denote the thresholds  $m_{H^+} = m_{\tilde{t}_i} + m_{\tilde{b}_j}$ ,  $i, j = 1, 2$ , see again Table 1.

The asymmetry  $A_P^{CP}$  reaches its maximum value at  $\tan\beta = 5$  and falls down

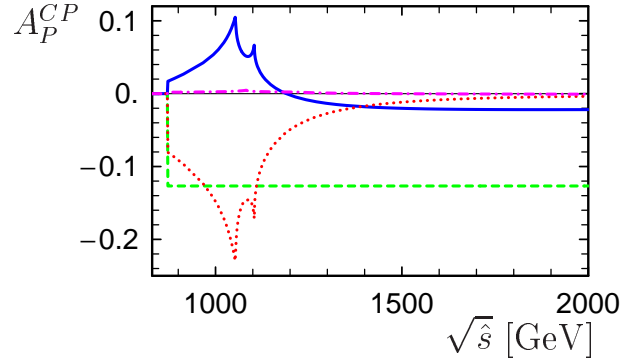


Figure 4: The contributions to the asymmetry  $A_P^{CP}$  at parton level for the chosen set of parameters (59) as a function of  $\sqrt{\hat{s}}$ ,  $m_{H^+} = 700$  GeV. The red dotted line corresponds to box graphs with a gluino, the solid blue one to the vertex graph with a gluino, the green dashed one to the  $W^\pm - H^\pm$  selfenergy graph with a  $\tilde{t}\tilde{b}$  loop, and the pink dash-dotted to the box and vertex graphs with  $\tilde{\chi}^{0/+}$ .

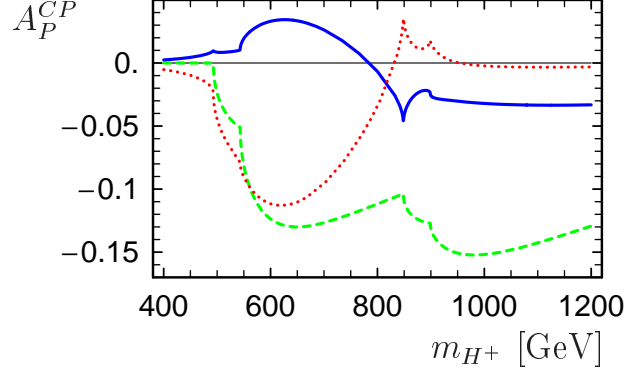


Figure 5: The contributions to the asymmetry  $A_P^{CP}$  at hadron level for the chosen set of parameters (59) as a function of  $m_{H^+}$ . The red dotted line corresponds to box graphs with a gluino, the solid blue one to the vertex graph with a gluino, and the green dashed one to the  $W^\pm - H^\pm$  selfenergy graph with a  $\tilde{t}\tilde{b}$  loop.

quickly with increasing  $\tan\beta$ . This dependence for  $m_{H^+} = 550$  GeV is shown on Fig. 6.

In Fig. 7 we present the dependence of  $A_P^{CP}$  as a function of  $M_{\tilde{Q}} (= M_{\tilde{U}} = M_{\tilde{D}})$ . The selfenergy contribution is first the biggest one, but it goes down to zero at  $M_{\tilde{Q}} \sim 467$  GeV because then the decay channel  $H^+ \rightarrow \tilde{t}_1 \tilde{b}_1$  closes. The kink at

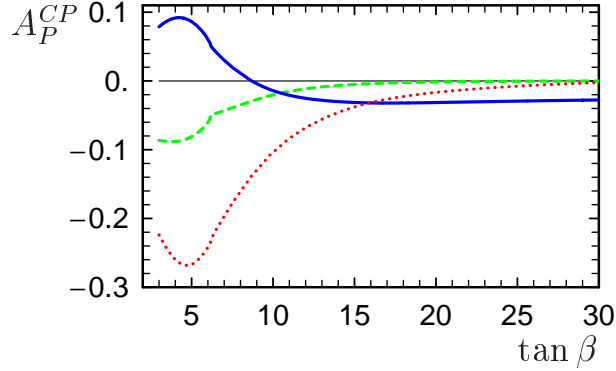


Figure 6: The contributions to the asymmetry  $A_P^{CP}$  at hadron level for the chosen set of parameters (59), but  $m_{\tilde{g}} = 450$  GeV, as a function of  $\tan \beta$ ,  $m_{H^+} = 550$  GeV. The red dotted line corresponds to box graphs with a gluino, the solid blue one to the vertex graph with a gluino, and the green dashed one to the  $W^\pm - H^\pm$  selfenergy graph with a  $\tilde{t}\tilde{b}$  loop.

$M_{\tilde{Q}} \sim 450$  GeV denotes the threshold  $H^+ \rightarrow \tilde{t}_1 \tilde{b}_2$ . The box contribution has its maximum of  $\sim 12\%$  at the threshold of  $H^+ \rightarrow \tilde{t}_1 \tilde{b}_1$

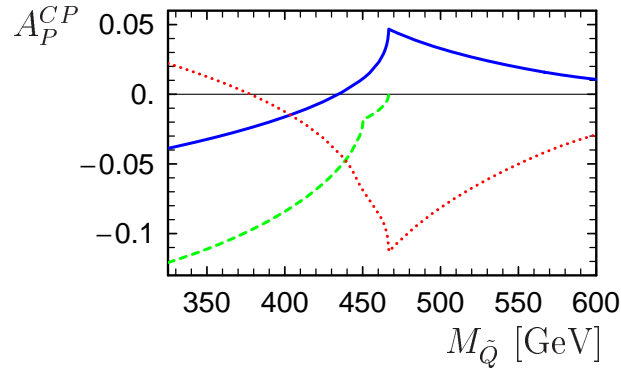


Figure 7: The contributions to the asymmetry  $A_P^{CP}$  at hadron level for the chosen set of parameters (59), but  $m_{\tilde{g}} = 435$  GeV, and  $m_{H^+} = 800$  GeV, as a function of  $M_{\tilde{Q}}$ . The red dotted line corresponds to box graphs with a gluino, the solid blue one to the vertex graph with a gluino, and the green dashed one to the  $W^\pm - H^\pm$  selfenergy graph with a  $\tilde{t}\tilde{b}$  loop.

In Fig. 8 the dependence of the three leading contributions to  $A_P^{CP}$  as a function



of  $m_{\tilde{g}}$  is shown for  $m_{H^+} = 550$  GeV. Of course, the selfenergy contribution is independent of the gluino mass, being about  $-8\%$ . The vertex contribution has a maximum and the box contribution a minimum at  $m_{\tilde{g}} \sim 425$  GeV, and then their absolute values decrease. The box contribution is at the minimum about  $-27\%$ .

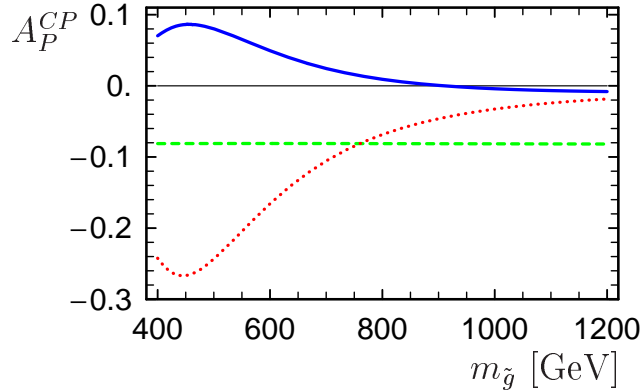


Figure 8: The contributions to the asymmetry  $A_P^{CP}$  at hadron level for the chosen set of parameters (59) as a function of  $m_{\tilde{g}}$ ,  $m_{H^+} = 550$  GeV. The red dotted line corresponds to box graphs with a gluino, the solid blue one to the vertex graph with a gluino, and the green dashed one to the  $W^\pm - H^\pm$  selfenergy graph with a  $\tilde{t}\tilde{b}$  loop.

## 5.2 Production and decay asymmetry

First we want to add a few remarks on the branching ratios (BR) of the relevant decays. Fig. 9 shows the tree-level BRs of  $H^\pm$  as functions of  $m_{H^+}$ . For small  $m_{H^+}$ , below the  $\tilde{t}\tilde{b}$  threshold, the dominant decay mode is  $H^\pm \rightarrow tb$ , with BR  $\approx 1$ , while the BR of  $H^\pm \rightarrow \nu\tau^\pm$  is of the order of a few percent, decreasing with increasing  $m_{H^+}$ . When the  $H^\pm \rightarrow \tilde{t}\tilde{b}$  channels are kinematically allowed, they start to dominate [21], and the BR of  $H^\pm \rightarrow \nu\tau^\pm$  to a good approximation becomes zero. However, the BR of  $H^\pm \rightarrow tb$  remains stable of the order of  $15 - 20\%$ . The BR of  $H^\pm \rightarrow W^\pm h^0$  reaches a few percent for small  $\tan\beta$  in a relatively narrow range of  $m_{H^+}$  [10]. In the considered range of parameters this decay is very much suppressed and we do not investigate it numerically.

In Fig. 10 we show the total production and decay asymmetry  $A_f^{CP}$  at hadron level, for  $f = tb$  and  $f = \nu\tau^\pm$ . Though for  $H^\pm \rightarrow \nu\tau^\pm$  it can go up to  $\sim 20\%$  for  $m_{H^+} \approx 650$  GeV, the BR of this decay in this range of  $H^\pm$  masses is too small and observation at LHC is impossible.

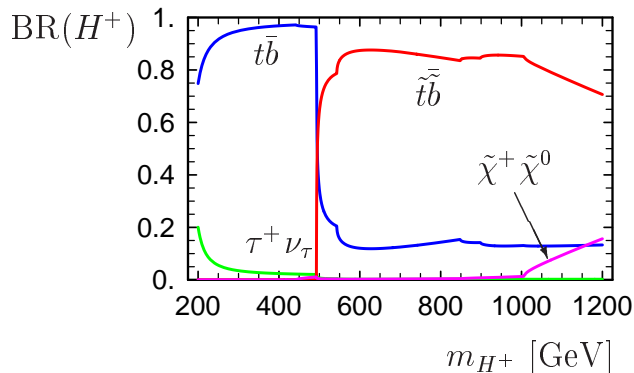


Figure 9: The tree-level branching ratios of  $H^+$  for the chosen set of parameters (59) as a function of  $m_{H^+}$ .

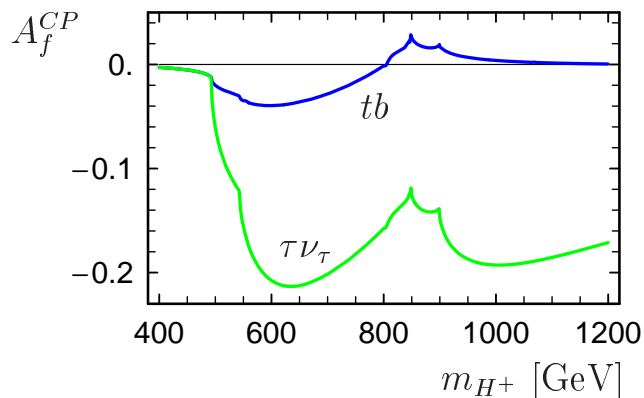


Figure 10: The total asymmetry  $A^{CP}$  at hadron level for the chosen set of parameters (59) as a function of  $m_{H^+}$ . The blue line corresponds to the case where  $H^\pm$  decays to  $tb$ , and the green one to  $H^\pm$  decay to  $\tau\nu_\tau$ .

As we have shown analytically, the total asymmetry in the production and decay is approximately the algebraic sum of the asymmetry in the production  $A_P^{CP}$ , and the asymmetry in the decay  $A_D^{CP}$ . One would think that the total CPV asymmetry will be large. Moreover, the CP-asymmetry in the decay alone is large [8].

Let us consider the subsequent decay  $H^\pm \rightarrow tb$  decay. In this case the contributions coming from the selfenergy graph with  $\tilde{t}\tilde{b}$  in the loop in the production and in the decay exactly cancel. This cancellation occurs in general for any possible  $H^\pm$  selfenergy loop contribution to the  $s$ - or  $t$ -channel. It can be easily shown by writing down the matrix element for the whole three particle final state process. As

an illustrative example, let us consider the contribution of both selfenergy graphs with  $\tilde{t}\tilde{b}$  from the production and from the decay, to the  $s$ -channel of our process, see Fig. 11. The matrix element, representing the sum of the two graphs in Fig. 11 reads

$$\mathcal{M}^{3,s} = -\frac{ig_s}{\hat{s}} \frac{g^2}{2} \bar{u}(p_b)(y_t P_R + y_b P_L)u(-p_t) \left[ (G_4)_{ij} \mathcal{R}_{L_i}^{\tilde{t}} \mathcal{R}_{L_j}^{\tilde{b}*} + (G_4)_{ij}^* \mathcal{R}_{L_i}^{\tilde{t}*} \mathcal{R}_{L_j}^{\tilde{b}} \right] \times \int_q \frac{(p_{\tilde{t}_i} + p_{\tilde{b}_j})^\mu (g_{\mu\nu} - \frac{p_{W_\mu} p_{W_\nu}}{m_W^2})}{(p_{H^+}^2 - m_{H^+}^2)(p_{\tilde{t}_i}^2 - m_{\tilde{t}_i}^2)(p_{\tilde{b}_j}^2 - m_{\tilde{b}_j}^2)(p_W^2 - m_W^2)} \bar{u}_s(p_t) \gamma^\nu P_L \not{p}_b T_{sr}^\alpha \gamma^\lambda u_r(p_b) \epsilon_\lambda^\alpha(p_g), \quad (60)$$

with  $\int_q = \int d^D q / (2\pi)^D$ ,  $p_{\tilde{t}_i} = p_{H^+} + q$  and  $p_{\tilde{b}_j} = q$ . It is clearly seen that (60) contains the sum of the couplings and their complex conjugate ones as a common factor. The expression in the box brackets at the end of the first row can be written as

$$(G_4)_{ij} \mathcal{R}_{L_i}^{\tilde{t}} \mathcal{R}_{L_j}^{\tilde{b}*} + (G_4)_{ij}^* \mathcal{R}_{L_i}^{\tilde{t}*} \mathcal{R}_{L_j}^{\tilde{b}} = 2\text{Re}[(G_4)_{ij} \mathcal{R}_{L_i}^{\tilde{t}} \mathcal{R}_{L_j}^{\tilde{b}}], \quad (61)$$

*i.e.* in this case the imaginary part of the couplings cancels. As the presence of a non zero imaginary part of the couplings is necessary for having CPV, it is clear that in this case the contribution of the selfenergy graphs on Fig. 11 to the CPV asymmetry is exactly zero. Our numerical study shows that the contributions of the vertex graphs from the production and from the decay also partially cancel with the box diagrams contribution. However, as the box graphs do not have an analogue in the decay, their contribution remains the leading one, see Fig. 12.

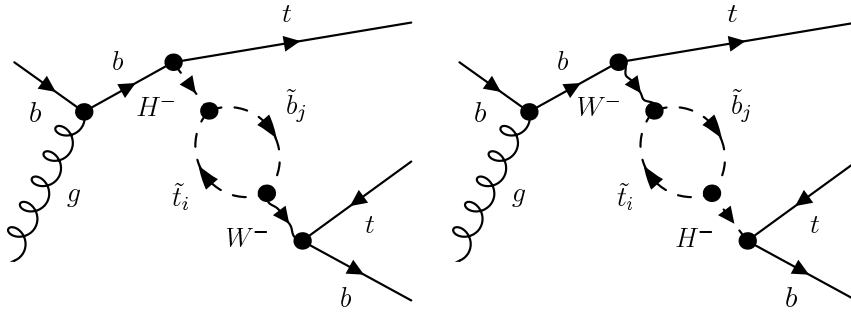


Figure 11: The selfenergy contributions with  $\tilde{t}\tilde{b}$  in the loop to the  $s$ -channel of the considered process, from the production and from the decay.

Fig. 13 shows the asymmetry in the production,  $A_P^{CP}$ , in the decay of  $H^\pm \rightarrow tb$ ,  $A_{D,tb}^{CP}$ , and the combined one,  $A_{tb}^{CP} = A_P^{CP} + A_{D,tb}^{CP}$ , as a function of the phase  $\phi_{A_t}$ . All three curves are symmetric for  $\phi_{A_t} \rightarrow -\phi_{A_t}$  because  $\phi_\mu = 0$ .  $A_P^{CP}$  and

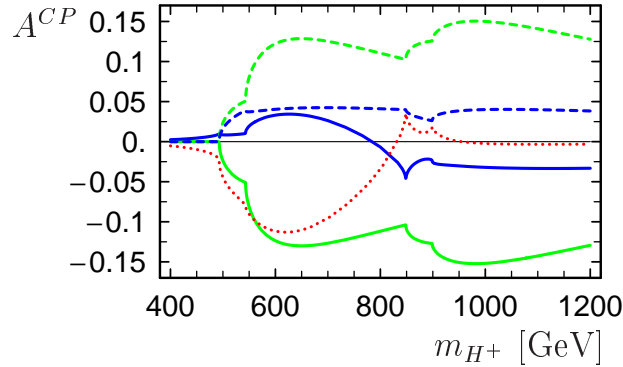


Figure 12: The contributions to the total asymmetry  $A_{tb}^{CP}$  at hadron level for the chosen set of parameters (59) as a function of  $m_{H^+}$ , with the same parameter set as used in Fig. 5. The dotted (red) line corresponds to box graphs with a gluino, the axially symmetric solid and dashed (green) lines correspond to the  $W^\pm - H^\pm$  selfenergy graph with a  $t\tilde{b}$  loop in the production and the decay, respectively, and the other two solid and dashed (blue) lines correspond to the vertex graph with a gluino, again in the production and the decay, respectively.

$A_{D,tb}^{CP}$  have negative relative signs with a maximum/minimum at  $|\phi_{A_t}| \lesssim 0.45\pi$ , with  $|A_P^{CP}| \sim 20\%$  and  $|A_{D,tb}^{CP}| \sim 16\%$  there. Due to this cancellation the resulting asymmetry  $A_{tb}^{CP}$  is reduced to  $\lesssim 4\%$ .

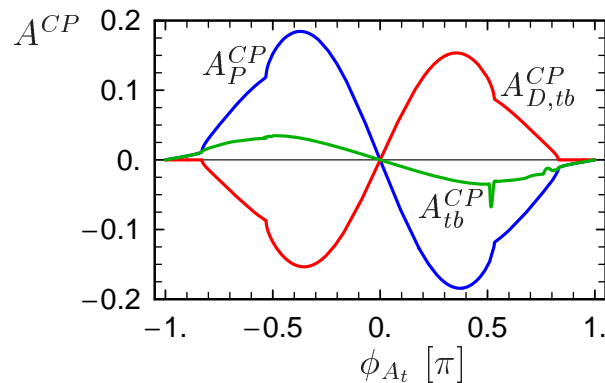


Figure 13: The asymmetry  $A^{CP}$  at hadron level for the production and the decay into  $tb$  only, and the total one, for the chosen set of parameters (59) as a function of  $\phi_{A_t}$ .

In order to avoid the cancellation, we can study the mass range of  $H^\pm$ , before the  $\tilde{t}_1\tilde{b}_1$  channel opens. In this case, having in mind our results in [8], the CP effects in the decay will be negligible and CPV will arise mainly in the production process due to the vertex and box contributions with  $\tilde{g}$  in the loops. For instance, for  $m_{H^+} = 400$  GeV and  $m_{\tilde{g}} = 450$  GeV we get  $A_{tb}^{CP} = -3\%$ .

In Fig. 14 the total asymmetries  $A_{tb}^{CP}$  and  $A_{\nu\tau}^{CP}$  as functions of  $m_{\tilde{g}}$  are shown for  $m_{H^+} = 550$  GeV. Both asymmetries are negative. They have their largest values at  $m_{\tilde{g}} \sim 425$  GeV, with  $A_{\nu\tau}^{CP} \sim -27\%$ ,  $A_{tb}^{CP} \sim -12\%$ , and then they decrease to zero.

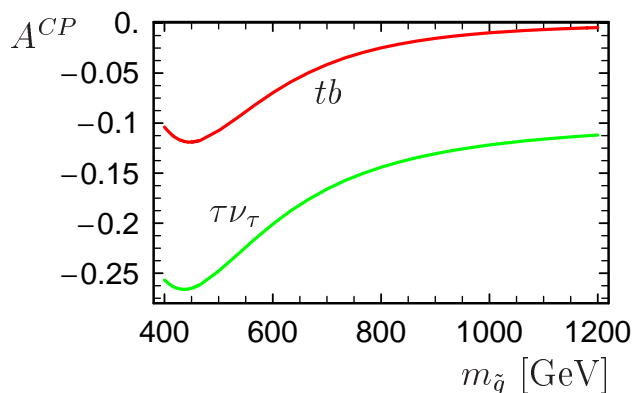


Figure 14: The total asymmetry  $A^{CP}$  at hadron level for the chosen set of parameters (59) as a function of  $m_{\tilde{g}}$ ,  $m_{H^+} = 550$  GeV. The (red) line denoted by  $tb$  corresponds to the case where  $H^\pm$  decays to  $tb$ , and the (green) one denoted by  $\tau\nu_\tau$  to  $H^\pm$  decay to  $\tau\nu_\tau$ .

In Fig. 15 the dependence of  $A_{tb}^{CP}$  on the absolute value of  $A_t$  is shown for three different values of  $m_{H^+}$ .

As already mentioned in the introduction, the phase of  $\mu$  is strongly constrained by the measurements of the EDMs. Nevertheless, we also studied the dependence of  $A^{CP}$  on  $\phi_\mu$ . Using  $\mu = 700 e^{-i\frac{\pi}{3}}$  GeV instead of  $\mu = -700$  GeV, we get for  $m_{\tilde{g}} = 450$  GeV in Fig. 14 the asymmetry  $A_{tb}^{CP} \sim -22\%$ .

The  $\tan\beta$  dependence is shown on Fig. 16, for  $f = tb$  and  $f = \tau\nu_\tau$ . In both considered cases the asymmetry  $A^{CP}$  has its maximum at  $\tan\beta \sim 5$ , with  $A_{tb}^{CP} \sim 12\%$  and  $A_{\nu\tau}^{CP} \sim 21\%$ . It approximately vanishes for  $\tan\beta \gtrsim 15$ .

We have compared our results with those in [13, 14]. Our numerical results are in good agreement with [13], but we disagree analytically and numerically with [14], where in addition the box contributions are missing.

The production rate of  $H^+$  at the LHC for  $m_{H^+} = 550$  GeV and  $\tan\beta = 5$  is  $\sim 15$  fb (including a K-factor from QCD of 1.5, see [22]), and the  $\text{BR}(H^+ \rightarrow tb)$

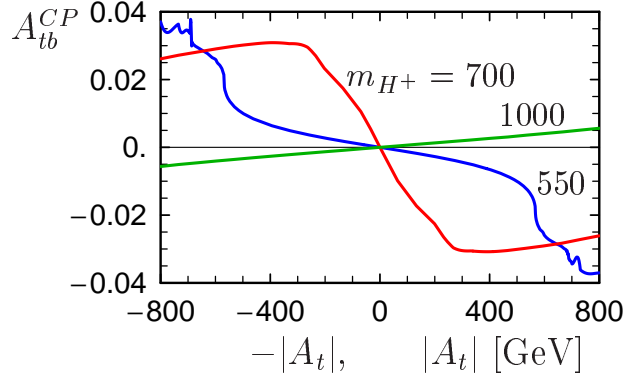


Figure 15: The total asymmetry  $A_{tb}^{CP}$  at hadron level for the chosen set of parameters (59) as a function of  $|A_t|$ , for three values of  $m_{H^+}$  (in GeV).

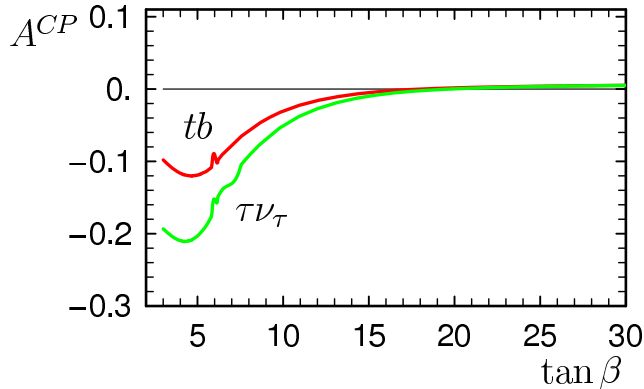


Figure 16: The total asymmetry  $A^{CP}$  at hadron level for the chosen set of parameters (59) as a function of  $\tan\beta$ ,  $m_{\tilde{g}} = 450$  GeV,  $m_{H^+} = 550$  GeV. The (red) line denoted by  $tb$  corresponds to the case where  $H^\pm$  decays to  $tb$ , and the (green) one denoted by  $\tau\nu_\tau$  corresponds to  $H^\pm$  decay to  $\tau\nu_\tau$ .

$\sim 20\%$ . For an integrated luminosity of  $200 \text{ fb}^{-1}$  we get  $N \sim 600$  and  $\sqrt{N} = 25$ . For  $m_{\tilde{g}} = 450$  we get  $A_{tb}^{CP} \sim 0.12$  and therefore the statistical significance  $\sqrt{N}A_{tb}^{CP} \sim 4$ . But because of the large background, the actual signal production rate will be most likely reduced and the statistical significance might be too low for a clear observation in  $H^\pm t$  production in the first stage of LHC. However, at SLHC with a design luminosity bigger by a factor of  $\sim 10$ , such a measurement would be worth of being performed.

## 6 Conclusions

The MSSM with complex parameters in particular with  $A_t$  complex, gives rise to CP violation in the production of  $H^\pm$ ,  $pp \rightarrow H^\pm t + X$ , and in the decays of  $H^\pm$  to  $tb$ ,  $\nu_\tau \tau^\pm$  and  $W^\pm h^0$  at one-loop level. We have calculated the corresponding asymmetries between the  $H^+$  and  $H^-$  rates both in the production and in the decays. A few improvements have been made with respect to previous calculations.

We have performed a detailed numerical analysis studying the dependence on the important parameters. A peculiarity is that in the case of  $pp \rightarrow H^\pm t + X$  with  $H^\pm \rightarrow tb$ , the contributions coming from the selfenergy graph with  $\tilde{t}\tilde{b}$  in the loop in the production and in the decay exactly cancel. Nevertheless, the asymmetry can go up to  $\sim 12\%$  for  $m_{H^+} \simeq 550$  GeV, mainly due to the box graphs with gluino in the production process. A measurement of the CP violating asymmetries at LHC can give important information of the parameters of the MSSM, especially on  $A_t$  and its phase.

## Acknowledgments

The authors acknowledge support from EU under the MRTN-CT-2006-035505 network programme. This work is supported by the "Fonds zur Förderung der wissenschaftlichen Forschung" of Austria, project No. P18959-N16. The work of E. C. and E. G. is partially supported by the Bulgarian National Science Foundation, grant 288/2008.

## A Masses and mixing matrices

The mass matrix of the stops in the basis  $(\tilde{t}_L, \tilde{t}_R)$  reads

$$\mathcal{M}_{\tilde{t}}^2 = \begin{pmatrix} M_{\tilde{Q}}^2 + m_Z^2 \cos 2\beta \left(\frac{1}{2} - \frac{2}{3} \sin^2 \theta_W\right) + m_t^2 & (A_t^* - \mu \cot \beta) m_t \\ (A_t - \mu^* \cot \beta) m_t & M_{\tilde{U}}^2 + \frac{2}{3} m_Z^2 \cos 2\beta \sin^2 \theta_W + m_t^2 \end{pmatrix}. \quad (62)$$

$\mathcal{M}_{\tilde{t}}^2$  is diagonalized by the rotation matrix  $\mathcal{R}^{\tilde{t}}$  such that  $\mathcal{R}^{\tilde{t}\dagger} \mathcal{M}_{\tilde{t}}^2 \mathcal{R}^{\tilde{t}} = \text{diag}(m_{\tilde{t}_1}^2, m_{\tilde{t}_2}^2)$  and  $\begin{pmatrix} \tilde{t}_L \\ \tilde{t}_R \end{pmatrix} = \mathcal{R}^{\tilde{t}} \begin{pmatrix} \tilde{t}_1 \\ \tilde{t}_2 \end{pmatrix}$ .

We have

$$\mathcal{R}^{\tilde{t}} = \begin{pmatrix} \mathcal{R}_{L1}^{\tilde{t}} & \mathcal{R}_{L2}^{\tilde{t}} \\ \mathcal{R}_{R1}^{\tilde{t}} & \mathcal{R}_{R2}^{\tilde{t}} \end{pmatrix} = \begin{pmatrix} e^{\frac{i}{2}\varphi_{\tilde{t}}} \cos \theta_{\tilde{t}} & -e^{\frac{i}{2}\varphi_{\tilde{t}}} \sin \theta_{\tilde{t}} \\ e^{-\frac{i}{2}\varphi_{\tilde{t}}} \sin \theta_{\tilde{t}} & e^{-\frac{i}{2}\varphi_{\tilde{t}}} \cos \theta_{\tilde{t}} \end{pmatrix}. \quad (63)$$

Analogously, the mass matrix of the sbottoms in the basis  $(\tilde{b}_L, \tilde{b}_R)$

$$\mathcal{M}_{\tilde{b}}^2 = \begin{pmatrix} M_{\tilde{Q}}^2 - m_Z^2 \cos 2\beta \left(\frac{1}{2} - \frac{1}{3} \sin^2 \theta_W\right) + m_b^2 & (A_b^* - \mu \tan \beta) m_b \\ (A_b - \mu^* \tan \beta) m_b & M_{\tilde{D}}^2 - \frac{1}{3} m_Z^2 \cos 2\beta \sin^2 \theta_W + m_b^2 \end{pmatrix}. \quad (64)$$

is diagonalized by the rotation matrix  $\mathcal{R}^{\tilde{b}}$  such that  $\mathcal{R}^{\tilde{b}\dagger} \mathcal{M}_b^2 \mathcal{R}^{\tilde{b}} = \text{diag}(m_{b_1}^2, m_{b_2}^2)$ .  $\mathcal{R}^{\tilde{b}}$  has the same structure like  $\mathcal{R}^{\tilde{t}}$  given with (63), and one can obtain it by making the interchange  $\tilde{t} \rightarrow \tilde{b}$ .

## B Interaction Lagrangian

The part of the MSSM interaction Lagrangian used in our analytical calculations is given in this section.

The interaction of the charged Higgs boson with two quarks reads

$$\mathcal{L}_{H^\pm tb} = H^+ \bar{t} (y_t P_L + y_b P_R) b + H^- \bar{b} (y_b P_L + y_t P_R) t, \quad (65)$$

where the  $P_L$  and  $P_R$  are the left/ right projection operators

$$P_L = \frac{1}{2}(1 - \gamma_5), \quad P_R = \frac{1}{2}(1 + \gamma_5), \quad (66)$$

$y_t$  and  $y_b$  are the tree-level couplings

$$y_t = h_t \cos \beta, \quad y_b = h_b \sin \beta, \quad (67)$$

with  $h_t$  and  $h_b$  - the top and bottom Yukawa couplings

$$h_t = \frac{g}{\sqrt{2}m_W} \frac{1}{\sin \beta}, \quad h_b = \frac{g}{\sqrt{2}m_W} \frac{1}{\cos \beta}. \quad (68)$$

The interaction of two quarks with gluon exchange is given by

$$\mathcal{L}_{qqg} = -g_s T_{ij}^a G_\mu^a \bar{q}_i \gamma^\mu q_j, \quad (69)$$

with  $i, j = 1, 2, 3$  and  $a = 1, \dots, 8$ .

The interaction of the charged Higgs boson with two squarks is described by

$$\mathcal{L}_{H^\pm \tilde{t}_i \tilde{b}_j} = (G_4)_{ij} H^+ \tilde{t}_i^* \tilde{b}_j + (G_4^*)_{ij} H^- \tilde{b}_j^* \tilde{t}_i, \quad (70)$$

with  $i, j = 1, 2$ ,

$$G_4 = \mathcal{R}^{\tilde{t}\dagger} \hat{G}_4 \mathcal{R}^{\tilde{b}}, \quad (71)$$

and the matrix  $\hat{G}_4$  is given by

$$\hat{G}_4 = \begin{pmatrix} h_b m_b \sin \beta + h_t m_t \cos \beta - \sqrt{2} g m_W \sin \beta \cos \beta & h_b (A_b^* \sin \beta + \mu \cos \beta) \\ h_t (A_t \cos \beta + \mu^* \sin \beta) & h_t m_b \cos \beta + h_b m_t \sin \beta \end{pmatrix}. \quad (72)$$

The  $W^\pm$ -squark-squark interaction Lagrangian reads

$$\mathcal{L}_{W^\pm \tilde{t}_i \tilde{b}_j} = -\frac{ig}{\sqrt{2}} (\mathcal{R}_{L_i}^{\tilde{t}} \mathcal{R}_{L_j}^{\tilde{b}*} W_\mu^- \tilde{b}_j^* \overleftrightarrow{\partial}^\mu \tilde{t}_i + \mathcal{R}_{L_i}^{\tilde{t}*} \mathcal{R}_{L_j}^{\tilde{b}} W_\mu^+ \tilde{t}_i \overleftrightarrow{\partial}^\mu \tilde{b}_j), \quad (73)$$



where  $i, j = 1, 2$  and  $A \overset{\leftrightarrow}{\partial}^\mu B = A (\partial_\mu B) - (\partial_\mu A) B$ .

The squark-quark-gluino interaction is given by

$$\begin{aligned} \mathcal{L}_{q\tilde{q}\tilde{g}} = & -\sqrt{2} g_s T_{jk}^a \left[ \tilde{g}_a (\mathcal{R}_{Li}^{\tilde{q}^*} e^{-\frac{i}{2}\phi_3} P_L - \mathcal{R}_{Ri}^{\tilde{q}^*} e^{\frac{i}{2}\phi_3} P_R) q^k \tilde{q}_i^{j*} \right. \\ & \left. + \tilde{q}^j (\mathcal{R}_{Li}^{\tilde{q}} e^{\frac{i}{2}\phi_3} P_R - \mathcal{R}_{Ri}^{\tilde{q}} e^{-\frac{i}{2}\phi_3} P_L) \tilde{g}_a \tilde{q}_i^k \right], \end{aligned} \quad (74)$$

with  $i = 1, 2, j, k = 1, 2, 3$ , and  $a = 1, \dots, 8$ .

The interaction of two quarks with W-boson exchange is described by

$$\mathcal{L}_{W^\pm tb} = -\frac{g}{\sqrt{2}} (W_\mu^+ \bar{t} \gamma^\mu P_L b + W_\mu^- \bar{b} \gamma^\mu P_L t). \quad (75)$$

## C Passarino-Veltman integrals

The definitions of the Passarino-Veltman two-, and three-point functions [23] in the convention of [24] and the derived analytical expressions for their imaginary parts [10, 25] are given in this section.

The PV two-point functions are defined through the 4-dimensional integrals, as

$$B_0(p_1^2, m_0^2, m_1^2) = \frac{1}{i\pi^2} \int d^D q \frac{1}{\mathcal{D}^0 \mathcal{D}^1}, \quad (76)$$

$$B_\mu(p_1^2, m_0^2, m_1^2) = \frac{1}{i\pi^2} \int d^D q \frac{q_\mu}{\mathcal{D}^0 \mathcal{D}^1} = p_{1\mu} B_1(p_1^2, m_0^2, m_1^2), \quad (77)$$

where we use the notation

$$\mathcal{D}^0 = q^2 - m_0^2 \quad \text{and} \quad \mathcal{D}^j = (q + p_j)^2 - m_j^2. \quad (78)$$

In the rest frame system of the (decaying) particle with impulse  $p_1$ , for the imaginary part of  $B_0$  we get

$$\text{Im } B_0(M_1^2, m_0^2, m_1^2) = \frac{\pi \lambda^{1/2}(M_1^2, m_0^2, m_1^2)}{M_1^2}, \quad (79)$$

where the  $\lambda$ -function is defined as

$$\lambda(x, y, z) = x^2 + y^2 + z^2 - 2xy - 2xz - 2yz. \quad (80)$$

In order to derive the imaginary part of  $B_1$  we use the relation

$$2k^2 B_1(k^2, m_0^2, m_1^2) = A_0(m_0^2) - A_0(m_1^2) + (m_1^2 - m_0^2 - k^2) B_0(k^2, m_0^2, m_1^2). \quad (81)$$

Having in mind that  $\text{Im } A_0(m^2) = 0$ , we obtain

$$\text{Im } B_1(M_1^2, m_0^2, m_1^2) = \frac{\pi(m_1^2 - m_0^2 - M_1^2) \lambda^{1/2}(M_1^2, m_0^2, m_1^2)}{2M_1^4}. \quad (82)$$

The PV three-point functions are defined as

$$\begin{aligned}
C_0(p_1^2, (p_1 - p_2)^2, p_2^2, m_0^2, m_1^2, m_2^2) &= \frac{1}{i\pi^2} \int d^D q \frac{1}{\mathcal{D}^0 \mathcal{D}^1 \mathcal{D}^2}, \\
C_\mu(p_1^2, (p_1 - p_2)^2, p_2^2, m_0^2, m_1^2, m_2^2) &= \frac{1}{i\pi^2} \int d^D q \frac{q_\mu}{\mathcal{D}^0 \mathcal{D}^1 \mathcal{D}^2} = p_{1\mu} C_1 + p_{2\mu} C_2.
\end{aligned} \tag{83}$$

For the absorptive parts of the integrals  $C_0, C_1$  and  $C_2$  in (83) in the rest frame of

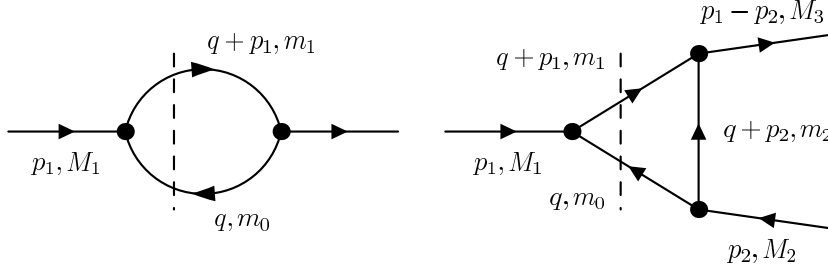


Figure 17: The selfenergy and vertex type diagrams corresponding to the PV two- and three-point integrals, when particles with masses  $m_0$  and  $m_1$  are on mass shell.

the (decaying) particle with momentum  $p_1$ , when particles with masses  $m_0$  and  $m_1$  are on mass shell, Fig. 17, we obtain

$$\text{Im } C_0(M_1^2, M_3^2, M_2^2, \mathbf{m}_0^2, \mathbf{m}_1^2, m_2^2) = -\frac{\pi}{\lambda^{1/2}(M_1^2, M_2^2, M_3^2)} \ln \left| \frac{a+b}{a-b} \right| \tag{84}$$

$$\text{Im } C_1(M_1^2, M_3^2, M_2^2, \mathbf{m}_0^2, \mathbf{m}_1^2, m_2^2) = \frac{M_2^2 A - (p_1 p_2) B}{\Delta} \tag{85}$$

$$\text{Im } C_2(M_1^2, M_3^2, M_2^2, \mathbf{m}_0^2, \mathbf{m}_1^2, m_2^2) = -\frac{(p_1 p_2) A - M_1^2 B}{\Delta} \tag{86}$$

Here we have

$$\begin{aligned}
\Delta &= M_1^2 M_2^2 - (p_1 p_2)^2, & (p_1 p_2) &= \frac{M_1^2 + M_2^2 - M_3^2}{2}, \\
a &= M_2^2 + m_0^2 - m_2^2 + 2 q^0 p_2^0, & b &= -2 |\vec{q}| |\vec{p}_2|, \\
A &= -\frac{\pi (m_1^2 - m_0^2 - M_1^2)}{2 \lambda^{1/2}(M_1^2, M_2^2, M_3^2)} \ln \left| \frac{a+b}{a-b} \right|, \\
B &= \frac{\pi}{\lambda^{1/2}(M_1^2, M_2^2, M_3^2)} \left\{ \frac{1}{2} (M_2^2 + m_0^2 - m_2^2) \ln \left| \frac{a+b}{a-b} \right| + 2 |\vec{q}| |\vec{p}_2| \right\}, \\
q^0 p_2^0 &= \frac{(m_1^2 - m_0^2 - M_1^2)(M_1^2 + M_2^2 - M_3^2)}{4 M_1^2}, \\
|\vec{q}| |\vec{p}_2| &= \frac{\lambda^{1/2}(M_1^2, m_0^2, m_1^2) \lambda^{1/2}(M_1^2, M_2^2, M_3^2)}{4 M_1^2}.
\end{aligned} \tag{87}$$

In (84)-(86) and further, we denote masses of the on-shell particles with bold font. Generally, the functions  $C_0, C_1$  and  $C_3$  have three terms according to the three possible cuts over the particles in the loops, and which of them is non zero depends on the kinematics. The imaginary part of  $C_0$  reads

$$\begin{aligned} \text{Im } C_0(M_1^2, M_3^2, M_2^2, m_0^2, m_1^2, m_2^2) &= \text{Im } C_0(M_1^2, M_3^2, M_2^2, \mathbf{m}_0^2, \mathbf{m}_1^2, m_2^2) + \\ &+ \text{Im } C_0(M_1^2, M_3^2, M_2^2, m_0^2, \mathbf{m}_1^2, \mathbf{m}_2^2) + \text{Im } C_0(M_1^2, M_3^2, M_2^2, \mathbf{m}_0^2, m_1^2, \mathbf{m}_2^2). \end{aligned} \quad (88)$$

In terms of the analytic formulas (84)-(86) we write

$$\begin{aligned} \text{Im } C_0(M_1^2, M_3^2, M_2^2, m_0^2, m_1^2, m_2^2) &= \text{Im } C_0(M_1^2, M_3^2, M_2^2, \mathbf{m}_0^2, \mathbf{m}_1^2, m_2^2) + \\ &+ \text{Im } C_0(M_3^2, M_1^2, M_2^2, m_2^2, \mathbf{m}_1^2, \mathbf{m}_0^2) + \text{Im } C_0(M_2^2, M_3^2, M_1^2, \mathbf{m}_0^2, m_2^2, \mathbf{m}_1^2). \end{aligned} \quad (89)$$

$$\begin{aligned} \text{Im } C_1(M_1^2, M_3^2, M_2^2, m_0^2, m_1^2, m_2^2) &= \text{Im } C_1(M_1^2, M_3^2, M_2^2, \mathbf{m}_0^2, \mathbf{m}_1^2, m_2^2) + \\ &+ \text{Im } C_1(M_3^2, M_1^2, M_2^2, m_2^2, \mathbf{m}_1^2, \mathbf{m}_0^2) + \text{Im } C_2(M_2^2, M_3^2, M_1^2, \mathbf{m}_0^2, m_2^2, \mathbf{m}_1^2), \end{aligned} \quad (90)$$

$$\begin{aligned} \text{Im } C_2(M_1^2, M_3^2, M_2^2, m_0^2, m_1^2, m_2^2) &= \text{Im } C_2(M_1^2, M_3^2, M_2^2, \mathbf{m}_0^2, \mathbf{m}_1^2, m_2^2) + \\ &+ [\text{Im } C_0(M_3^2, M_1^2, M_2^2, m_2^2, \mathbf{m}_1^2, \mathbf{m}_0^2) + \text{Im } C_1(M_3^2, M_1^2, M_2^2, m_2^2, \mathbf{m}_1^2, \mathbf{m}_0^2) + \\ &+ \text{Im } C_2(M_3^2, M_1^2, M_2^2, m_2^2, \mathbf{m}_1^2, \mathbf{m}_0^2)] + \text{Im } C_1(M_2^2, M_3^2, M_1^2, \mathbf{m}_0^2, m_2^2, \mathbf{m}_1^2). \end{aligned} \quad (91)$$

## References

- [1] M. Dugan, B. Grinstein and L. J. Hall, Nucl. Phys. B **255** (1985) 413.
- [2] M. Carena, M. Quiros and C. E. Wagner, Nucl. Phys. B **524** (1998) 3 [hep-ph/9710401]; for a review see: A. G. Cohen, D. B. Kaplan and A. E. Nelson, Ann. Rev. Nucl. Part. Sci. **43** (1993) 27 [hep-ph/9302210].
- [3] I. S. Altarev *et al.*, Phys. Lett. B **276** (1992) 242; I. S. Altarev *et al.*, Phys. Atom. Nucl. **59** (1996) 1152 [Yad. Fiz. **59N7** (1996) 1204]; E. D. Commins, S. B. Ross, D. DeMille and B. C. Regan, Phys. Rev. A **50** (1994) 2960.
- [4] P. Nath, Phys. Rev. Lett. **66** (1991) 2565; Y. Kizukuri and N. Oshimo, Phys. Rev. D **46** (1992) 3025; R. Garisto and J. D. Wells, Phys. Rev. D **55** (1997) 1611 [hep-ph/9609511]; Y. Grossman, Y. Nir and R. Rattazzi, Adv. Ser. Direct. High Energy Phys. **15** (1998) 755 [hep-ph/9701231].
- [5] A. Pilaftsis, Phys. Rev. D **58** (1998) 096010 [hep-ph/9805373] and Phys. Lett. B **435** (1998) 88 [hep-ph/9805373]; A. Pilaftsis and C. E. Wagner, Nucl. Phys. B **553** (1999) 3 [hep-ph/9902371]; D. A. Demir, Phys. Rev. D **60** (1999) 055006 [hep-ph/9901389].

- [6] M. Carena, J. R. Ellis, A. Pilaftsis and C. E. Wagner, Nucl. Phys. **B 586** (2000) 92 [hep-ph/0003180].
- [7] For a review, see D. Atwood, S. Bar-Shalom, G. Eilam and A. Soni, Phys. Rept. **347** (2001) 1 [hep-ph/0006032].
- [8] E. Christova, H. Eberl, E. Ginina, W. Majerotto, JHEP **0702** (2007) 075 [hep-ph/0612088].
- [9] E. Christova, H. Eberl, S. Kraml and W. Majerotto, JHEP **0212** (2002) 021 [hep-ph/0211063].
- [10] E. Christova, E. Ginina, M. Stoilov JHEP **11** (2003) 027 [hep-ph/0307319].
- [11] E. Ginina, contribution to the 4th workshop "Gravity, Astrophysics, and Strings at the Black Sea", 2007, hep-ph/0801.2344
- [12] E. Christova, H. Eberl, E. Ginina, arXiv:0812.0265 [hep-ph].
- [13] J. William, contributions to CPNSH Report, CERN-2006-009 (hep-ph/0608079)
- [14] Kang Young Lee, Dong-Won Jung, H. S. Song, Phys. Rev. D **70** (2004) 117701 [hep-ph/0307246].
- [15] N. Kidonakis, JHEP **0505** (2005) 011, [hep-ph/0412422].
- [16] E. Christova, H. Eberl, S. Kraml and W. Majerotto, Nucl. Phys. B **639** (2002) 263; E. Christova, H. Eberl, S. Kraml and W. Majerotto, Erratum to Nucl. Phys. B **639** (2002) 263.
- [17] T. Hahn, Nucl. Phys. Proc. Suppl. B **89** (2000) 231; T. Hahn, *FeynArts User's Guide*, Comp. Phys. Commun. **140** (2001) 418; T. Hahn, M. Perez-Victoria, *FormCalc User's Guide*, Comput. Phys. Commun. **118** (1999) 153; T. Hahn, M. Perez-Victoria, *LoopTools User's Guide*, Comput. Phys. Commun. **118** (1999) 153. (The software and all manuals are available at <http://www.feynarts.de>.)
- [18] G. J. van Oldenborgh, Comput. Phys. Commun. **66** (1991) 1.
- [19] J. Pumplin, D.R. Stump, J. Huston, H.L. Lai, Pavel M. Nadolsky, W.K. Tung, JHEP **12** (2002) 0207 [hep-ph/0201195].
- [20] M. Battaglia et al., Eur. Phys. J. C **22** (2001) 535, [arXiv:hep-ph/0106204].
- [21] A. Bartl, K. Hidaka, Y. Kizukuri, T. Kon, W. Majerotto, Phys. Lett. B **315** (1993) 360.

- [22] A. Belyaev, D. Garcia, J. Guasch and J. Sola, hep-ph/0203031.
- [23] G. Passarino and M. J. Veltman, Nucl. Phys. B **160** (1979) 151.
- [24] A. Denner, Fortschr. Phys. **41** (1993) 307.
- [25] M. Frank, I. Turan, Phys. Rev. D **76** (2007) 016001, [hep-ph/0703184].